Submitted to the Astrophysical Journal
Preprint typeset using LaTeX style emulateapj v. 5/2/11

arXiv:1412.2327v2 [astro-ph.SR] 17 Dec 2014

THE FIRST "WATER FOUNTAIN" COLLIMATED OUTFLOW IN A PLANETARY NEBULA

José F. Gómez[1], Olga Suárez[2], Philippe Bendjoya[2], J. Ricardo Rizzo[3], Luis F. Miranda[1,4], James A. Green[5,6], Lucero Uscanga[7], Enrique García-García[3], Eric Lagadec[2], Martín A. Guerrero[1], Gerardo Ramos-Larios[8]

Submitted to the Astrophysical Journal

ABSTRACT

"Water fountains" (WFs) are evolved objects showing high-velocity, collimated jets traced by water maser emission. Most of them are in the post-Asymptotic Giant Branch and they may represent one of the first manifestations of collimated mass loss in evolved stars. We present water maser, carbon monoxide, and mid-infrared spectroscopic data (obtained with the Australia Telescope Compact Array, Herschel Space Observatory, and the Very Large Telescope, respectively) toward IRAS 15103−5754, a possible planetary nebula (PN) with WF characteristics. Carbon monoxide observations show that IRAS 15103−5754 is an evolved object, while the mid-IR spectrum displays unambiguous [NeII] emission, indicating that photoionization has started and thus, its nature as a PN is confirmed. Water maser spectra show several components spreading over a large velocity range ($\simeq$ 75 km s^{-1}) and tracing a collimated jet. This indicates that the object is a WF, the first WF known that has already entered the PN phase. However, the spatial and kinematical distribution of the maser emission in this object are significantly different from those in other WFs. Moreover, the velocity distribution of the maser emission shows a "Hubble-like" flow (higher velocities at larger distances from the central star), consistent with a short-lived, explosive mass-loss event. This velocity pattern is not seen in other WFs (presumably in earlier evolutionary stages). We therefore suggest that we are witnessing a fundamental change of mass-loss processes in WFs, with water masers being pumped by steady jets in post-AGB stars, but tracing explosive/ballistic events as the object enters the PN phase.

Subject headings: masers; planetary nebulae: general; planetary nebulae: individual IRAS 15103−5754; stars: AGB and post-AGB; stars: mass-loss; stars: winds, outflows

1. INTRODUCTION

"Water fountain" (WF) stars are low- to intermediate-mass stars ($<$ 8 M$_\odot$) evolved objects that show collimated jets traced by high-velocity water masers at 22 GHz (see Imai 2007; Desmurs 2012, for reviews). The velocity spread in their water maser spectra is typically $\geq$ 75 km s^{-1}, and can be as large as $\simeq$ 500 km s^{-1} (Gómez et al. 2011). These velocities indicate the presence of motions faster than the typical expansion velocities in spherical AGB envelopes, of $\simeq 10-20$ km s^{-1}, as traced by double-peaked OH maser spectra (with velocity separations between both components of $\simeq 20-40$ km s^{-1}, te Lintel Hekkert et al. 1989). Most WFs are in the short transition phase between the Asymptotic Giant Branch (AGB) and the planetary nebula (PN) stage. Their being in this particular evolutionary stage, together with the short dynamical ages of the maser outflows (5-100 yr; Imai 2007), and their relatively strong optical obscuration (Suárez et al. 2008) indicate that WFs may represent one of the first manifestations of collimated mass-loss in evolved stars of low and intermediate mass.

There is growing consensus that the action of collimated jets on the circumstellar envelope during the post-AGB phase will determine the shape of PNe once photoionization starts (Sahai & Trauger 1998; Bujarrabal et al. 2001). Therefore, WFs are key objects to understand when and how the spherical symmetry seen in AGB stars and earlier stages is broken to give rise to the spectacular variety of morphologies displayed in the PN phase.

Only 16 sources have been identified so far as possible WFs (Desmurs 2012; Vlemmings et al. 2014). Fourteen of them seem to be in the post-AGB phase. Of the remaining two candidates, the source W43A may be at the late AGB stage (Imai et al. 2002). At the other end of the age spectrum, Suárez et al. (2009) detected a WF candidate toward the source IRAS 15103−5754 (hereafter I15103), which had been classified as a possible PN (van de Steene & Pottasch 1993). If confirmed, this would be the first known PN with WF characteristics. This confirmation is important, since it would prove that collimated jets with enough energy to pump maser emission can persist after the star enters the PN phase. Such a jet could contribute to the shaping of the nebula while photoionization already proceeds.

I15103 is an optically obscured object (Suárez et al.

[1] Instituto de Astrofísica de Andalucía, CSIC, Glorieta de la Astronomía s/n, E-18008, Granada, Spain
[2] Laboratoire Lagrange, UMR 7293, Université de Nice Sophia-Antipolis, CNRS, Observatoire de la Côte d'Azur, 06304, Nice, France
[3] Centro de Astrobiología (INTA-CSIC), Ctra. M-108, km. 4, E-28850 Torrejón de Ardoz, Spain
[4] Universidad de Vigo, Departamento de Física aplicada, Facultad de Ciencias, Campus Lagoas-Marcosende s/n, 36310, Vigo, Spain
[5] CSIRO Astronomy and Space Science, Australia Telescope National Facility, PO Box 76, Epping, NSW 1710, Australia
[6] SKA Organisation, Jodrell Bank Observatory, Lower Withington, Macclesfield SK11 9DL, UK
[7] Institute of Astronomy, Astrophysics, Space Applications and Remote Sensing, National Observatory of Athens, 15236 Athens, Greece
[8] Instituto de Astronomía y Meteorología, Av. Vallarta No. 2602, Col. Arcos Vallarta, C.P. 44130 Guadalajara, Jalisco, Mexico

2006; Ramos-Larios et al. 2012) that shows a bipolar morphology in near and mid-infrared images (Ramos-Larios et al. 2012; Lagadec et al. 2011). Its classification as a PN was based on the presence of radio continuum emission (van de Steene & Pottasch 1993), which is typically seen in the photoionized regions of these objects. However, the radio continuum flux density decreases at higher frequencies (Urquhart et al. 2007a; Suárez et al. 2014), which is indicative of non-thermal emission and cannot be attributed to free-free processes in a photoionized region. The time-evolution of its non-thermal emission has been attributed to the onset of photoionization (Suárez et al. 2014). However, to date there is no conclusive evidence that I15103 has already entered the PN phase or even that it is an evolved object.

In this paper, we provide solid evidence that I15103 is a bona fide WF, and that it is also PN. Our observations are presented in Sec. 2. In Sec. 3 we present and discuss our results, and we summarize our conclusions in Sec. 4

2. OBSERVATIONS

2.1. *Australia Telescope Compact Array*

Observations at 1.3 cm were carried out with the Australia Telescope Compact Array[9] (ATCA) on 2011 August 11 and 2012 October 23, under observing projects C2315 and C2746, respectively. We used the Compact Array Broadband Backend (CABB), which provides two independent bands of 2 GHz each, in dual linear polarization. We centered these bands at 22 and 24 GHz. The observations on 2011 were carried out in the H168 array configuration (including antenna C06, located at 6 km from the array center), and used the 64M mode of CABB, which samples each 2 GHz bandpass into 32 frequency channels of 64 MHz. Observations on 2012 October were carried out in the H214 array configuration (without antenna C06) and used the 1M mode, which samples 2048 channels, each of them 1 MHz wide. In addition to this broad band mode (whose data were presented in Suárez et al. 2014), we observed the emission of the $6_{16}-5_{23}$ transition of H_2O (rest frequency = 22235.08 MHz), using the zooming capabilities of CABB: on 2011 August, one of the wideband channels (64 MHz width) was subdivided into 2048 spectral-line channels, providing a velocity resolution of $\simeq 0.42$ km s^{-1}, and a total coverage of $\simeq 860$ km s^{-1}, while on 2012 October, we combined 16 wideband channels (1 MHz width), spaced by 0.5 MHz, and each subdivided into 2048 spectral-line channels, thus providing a velocity resolution of $\simeq 6.6 \times 10^{-3}$ km s^{-1}, and a total coverage of $\simeq 114$ km s^{-1}. For the latter epoch of observations, spectral line data presented in this paper were smoothed up to a velocity resolution of $\simeq 0.066$ km s^{-1} in our data reduction.

The absolute flux, bandpass, and complex gains were calibrated with sources PKS 1934-638, PKS 1921-293, and PKS 1613-586, respectively. Initial calibration and imaging was carried out with standard procedures using MIRIAD (Sault & Killeen 2004). Continuum was subtracted from line data with task UVLIN of MIRIAD. Then, we selected the spectral-line channel with the highest flux density, and applied self-calibration with the AIPS package of NRAO. The derived amplitude and phase corrections were then applied to the whole line dataset. A new narrow-band continuum dataset at $\simeq 22$ GHz was obtained by averaging the line-free channels from this self-calibrated dataset. Since these narrow-band continuum data share the same corrections as obtained for the self-calibration of the maser line, the systematic astrometric errors and those due to atmospheric phase variations are the same in line and continuum. In this way, we can ascertain the relative position between the maser components and the maximum of the continuum emission with an accuracy which is only limited by the noise in the images. Under these conditions, the 1-sigma positional accuracy between the continuum and the maser components (and among the different maser components) can be quantified as $\sigma_{\rm pos} \simeq \theta/(2 \times {\rm snr})$, where θ is the source size in the image (i.e., the synthesized beam in the case of point sources), and snr is the signal-to-noise ratio. Considering maser components > 1 Jy, these accuracies were typically better than $\simeq 30$ and 25 milliarcsec between maser and continuum for our data on 2011 and 2012, respectively, and $\simeq 1$ and 20 milliarcsec among maser components, for 2011 and 2012 data, respectively.

Final images of line and continuum emission were obtained with a robust weighting of visibilities, using a robust parameter 0 in task IMAGR of AIPS. Synthesized beam sizes were $\simeq 3.1'' \times 1.1''$ (position angle $= 0^\circ$) and $10.0'' \times 7.0''$ (position angle $= 64^\circ$) in 2011 and 2012, respectively.

2.2. *Herschel Space Observatory*

I15103 was included as one of the targets of *Herschel* Space Observatory[10] (Pilbratt et al. 2010) in the first open time period (Proposal ID: OT1_jrizzo_1). The CO observations were obtained using the Heterodyne Instrument for the Far-Infrared (HIFI) (de Graauw et al. 2010). We present here the first analysis of the CO $J = 5 \rightarrow 4$ (567.2684 GHz, band 1) and $10 \rightarrow 9$ (1151.985 GHz, band 5) spectra. Full width at half maximum (FWHM) of the telescope beam is estimated to be $44''$ and $19''$ at these bands, respectively.

The observations were gathered in two orthogonal lineal polarizations. The receiver worked in double sideband (DBS) mode, which allowed the use of both lower- and upper-side bands simultaneously. The observing mode was dual beam switching, with the emission-free position $3'$ away from the source position. We used the HIFI wide-band spectrometer (WBS), which provides four adjacent bands per polarization with an instantaneous width of 1 GHz each.

The spectra were initially processed using HIPE (*Herschel* Interactive Processing Environment), version 11.0.1, and exported to CLASS[11] using the hiClass tool within HIPE. Each 1-GHz individual band was concatenated providing 2 individual spectra (one per polarization) of 4 GHz total bandwidth. The original frequency spacing was 500 kHz, although the effective spectral resolution was $\simeq 1.1$ MHz. A baseline of low order was fitted,

[9] The Australia Telescope is funded by the Commonwealth of Australia for operation as a National Facility managed by CSIRO

[10] *Herschel* is an ESA space observatory with science instruments provided by European-led Principal Investigator consortia and with important participation from NASA.

[11] GILDAS software. http://www.iram.fr/IRAMFR/GILDAS/

and there was no evidence of significant standing waves. Spectra have been converted to a main-beam brightness temperature scale ($T_{\rm mb}$), by assuming main beam efficiencies of 0.76 and 0.64 for bands 1 and 5, respectively (Roelfsema et al. 2012).

After spectral Hanning smoothing, the resulting spectra we present in this paper have 1σ rms noises of 55 mK and 52 mK, and velocity resolutions of 3.1 km s^{-1} and 4.7 km s^{-1} for the CO $J = 5 \rightarrow 4$ and $10 \rightarrow 9$ transitions, respectively.

2.3. *Very Large Telescope*

A mid-infrared, N-band (8-13 μm) spectrum with spectral resolution of 300 was taken toward I15103 on 2009 June 24 with the VLT spectrometer and imager for the mid–infrared (VISIR) instrument (Lagage et al. 2004), mounted on the Very Large Telescope (VLT) UT3. The slit (with a length of 32″ and width of 0.4″) was centered on the object and aligned along the major axis of the nebula, with a position angle of 45°. The classical chopping and nodding technique was used to remove the sky background, using a parallel chopping with a frequency of 0.25 Hz and a "chop throw" of 10″. To cover the full N band window, we used four gratings centered at 8.5, 9.8, 11.4, and 12.2 μm. We used detector integration times of 0.2 seconds and a total integration time of 180 seconds per grating. In order to remove telluric lines, we observed the mid-infrared standard star HD 111915 with exactly same settings immediately after the I15103 observations. Data reduction was performed using Gasgano (v2.4.5; Izzo et al. 2004).

3. RESULTS AND DISCUSSION

3.1. *Radio continuum emission*

Both broad-band (Suárez et al. 2014) and narrow-band continuum (this paper) images show an unresolved source of emission at 22 GHz, located at R.A.(J2000) = $15^h14^m17.94^s$, Dec(J2000) = −58°05′21.9″ (absolute positional error $\simeq 0.6''$), with a flux density of $\simeq 35 \pm 5$ mJy. The narrow-band continuum images were used to determine the relative position of the maser components with respect to the continuum emission, with a high accuracy (as mentioned in Section 2.1). Suárez et al. (2014) have confirmed that the radio continuum emission is non-thermal, and its spectral index has significantly varied over the past few years. The non-thermal emission traces the motion of electrons, accelerated by shocks, within a magnetic field, and the variation of spectral index has been interpreted by Suárez et al. (2014) as the result of the onset of photoionization.

The highest angular resolution in our observations is of $\simeq 3'' \times 1''$, which is larger than the extent of the infrared lobes of the nebula (Lagadec et al. 2011), so we cannot accurately determine the exact location and extent of this non-thermal emission. However, assuming that mass-loss processes are symmetrical with respect to the central star, the position of the unresolved radio continuum emission provides an estimate of the location of the star.

3.2. *The outflow traced by water masers*

Maser emission was detected in both epochs, with multiple components spanning over a velocity range of up to $\simeq 75$ km s^{-1} (Fig. 1 and Table 1). In 2011 the peak emission was extraordinarily intense, reaching 1.731 kJy. The data on 2011 (which provides the highest positional accuracy) show that most of the maser components are aligned with the radio continuum position on a linear distribution (Fig. 2), along a position angle of $\simeq 56°$ (measured from north to east). Four additional components show a parallel linear distribution, offset $\simeq 0.14''$ south east of the radio continuum position. Four maser components depart from these main "strings", and they could be part of a different structure (like an equatorial torus), but they are the weakest ones and, hence, their positional accuracy is lower. Therefore, a significant fraction of the water maser emission seems to trace a high-velocity, collimated ejection, which confirms its nature as a water fountain. The direction of the water maser linear distribution is almost coincident with that of the lobes detected in the IR images (Lagadec et al. 2011, see Fig. 2) and presents an extension of 0.4″ from the center of the PN, equivalent to 440 AU assuming a kinematical distance of 1.1 kpc (near kinematical distance for a $V_{\rm LSR} \simeq -23$ km s^{-1}, see below, and assuming the model by Reid et al. 2009, without applying the correction for high-mass star-forming regions). The high velocities of the maser components (total velocity spread $\simeq 75$ km s^{-1}), together with the small spatial extent of the structure they trace, suggest that the collimated ejection is extremely young. However, with the information on LSR velocity and projected size alone it is impossible to obtain an accurate estimate of the dynamical age of the outflow. For an age estimate, we would need proper motion measurements, or an accurate determination of the distance and the inclination angle with respect to the observer.

In Fig. 2 we can see that the maser emission shows a Hubble-flow pattern, i.e., a linear dependence of velocity on distance from the radio continuum position, with increasing relative velocities at larger distances. This linear trend gives us an estimate of $\simeq -23$ km s^{-1} for the (LSR) radial velocity of the central star (the intersect velocity of the linear fit at spatial offset = 0), and indicates that most components are blueshifted with respect to it. This blueshifted bias might represent an intrinsic asymmetry in the ejection, but it is more likely to be an effect of maser amplification, since the approaching side would have the radio continuum in the background along the line of sight. Maser emission will then be favored on that side, since it amplifies a stronger background than in the redshifted side. A blueshifted bias is also seen in OH maser emission from PNe (Uscanga et al. 2012) and high-mass young stellar objects (YSOs) (Caswell & Green 2011), and it may have the same physical origin.

The observed kinematical pattern (the Hubble-like flow) is common in spectroscopic data at optical/infrared wavelengths (e.g., Corradi & Schwarz 1993; Meaburn et al. 2005, 2008; Hrivnak et al. 2008) and CO molecular lines (Bujarrabal et al. 1997; Alcolea et al. 2001) of bipolar PNe and post-AGB stars. However, it is not clearly present in water maser jets of post-AGB WFs (Imai et al. 2002, 2004; Boboltz & Marvel 2005; Gómez et al. 2011). Several models have been proposed to explain these linear velocity gradients in PNe and post-AGB stars (Dennis et al. 2008; Soker & Kashi 2012;

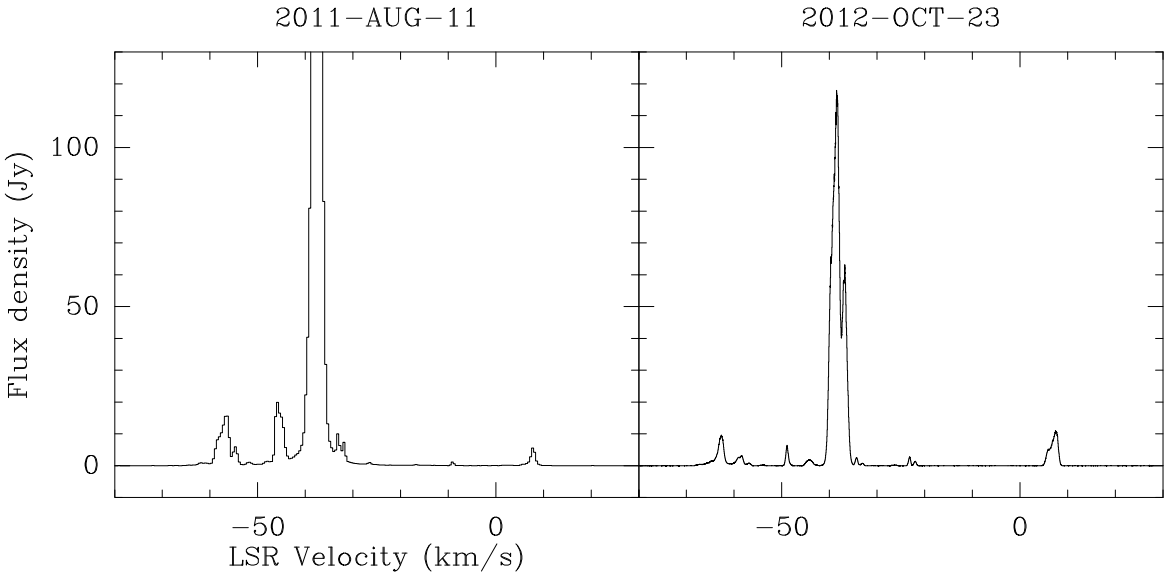

Figure 1. Water maser spectra toward I15103, in two different epochs, integrating over the whole emitting region. The component with the highest flux density (1.731 kJy) in the left panel has been truncated, so that weaker components can be seen.

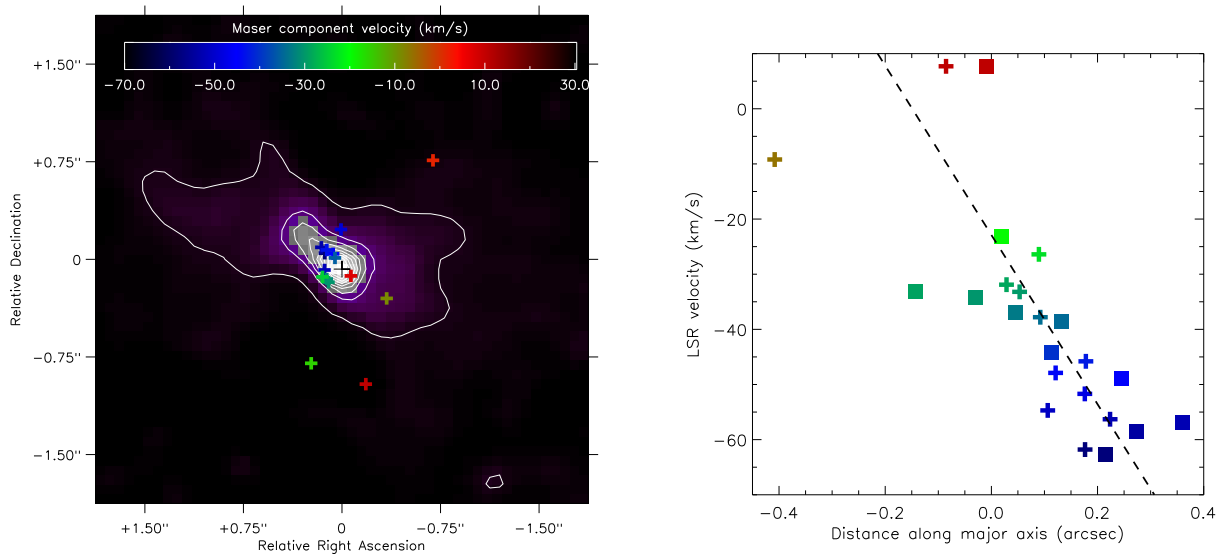

Figure 2. Left: Water maser components (colored crosses) in the 2011 August data, plotted on an image the 12.81 μm ([Ne II] filter) presented by Lagadec et al. (2011). The color scale of the crosses represent the LSR velocity of the components. Coordinates are offsets with respect to the position of the radio continuum emission (marked with a black cross). The alignment between the radio data and the mid-IR image has been made assuming that the intensity peak of the latter coincides with the position of the radio continuum emission. Right: LSR velocity of the maser components vs. projected distance to the radio continuum emission, along the major axis of the maser structure (P.A. = 56°). Crosses and closed squares represent the data on 2011 and 2012, respectively. Color code is the same as in the right panel. The dashed line represents the best linear fit to the plotted data, with distances weighted by the inverse squared positional uncertainty of each point.

Akashi & Soker 2013; Balick et al. 2013) but all point to short-lived, explosive/ballistic mass-loss events rather than to the presence of steady jets. On the other hand, the large velocity gradients of an explosive event could in principle make the presence of maser emission difficult, as this emission requires a significant amplification path with coherent velocities along the line of sight. A possibility for its detection in I15103 is that the mass loss traced by the maser emission consists of discrete parcels of gas (i.e., bullets) ejected in an explosive event. The gas of each parcel would have the required velocity coherence to produce maser emission.

3.3. *Confirmation of the nature of IRAS 15103−5754 as a planetary nebula*

It is often difficult to ascertain whether an object is a PN. Such a classification requires different observations to discard that it could be a YSO or an evolved star in a phase previous to photoionization (AGB or post-AGB), since all these types of objects share many observational characteristics. Visible images and spectra of Hα and [OIII] emission are useful diagnostic tools. However, I15103 is not visible at optical wavelengths (Suárez et al. 2006). In particular, Hα images do not show any emission toward the source position. For such a deeply obscured object, infrared and radio data must

Table 1
Water maser components in IRAS 15103−5754

$V_{\rm LSR}$ (km s^{-1})	S_ν (Jy)	Δ_{ra} (mas)	Δ_{dec} (mas)	σ_p (mas)
	2011 August 11			
−61.8	0.890 ± 0.007	131	122	4
−56.8	14.200 ± 0.009	157.0	167.2	0.3
−54.7	3.918 ± 0.009	132.6	−6.8	1.1
−51.7	0.695 ± 0.007	7	304	5
−47.9	1.422 ± 0.007	67.0	117.2	2.2
−45.8	11.847 ± 0.010	115.7	147.0	0.4
−37.8	1731.1 ± 0.3	53.20	86.00	0.09
−33.2	7.823 ± 0.010	115.6	−76.4	0.6
−31.9	4.885 ± 0.008	102.3	−101.0	0.8
−26.4	0.622 ± 0.007	148	−60	5
−16.7	0.287 ± 0.007	234	−724	11
−9.2	0.589 ± 0.007	−340	−225	6
1.4	0.133 ± 0.006	−692	836	22
7.7	3.580 ± 0.007	−67.8	−52.2	1.0
11.1	0.088 ± 0.006	−182	−884	30
	2012 October 23			
−62.66	9.708 ± 0.016	188	108	4
−58.47	3.107 ± 0.014	192	198	12
−56.88	0.802 ± 0.009	221	303	30
−54.00	0.231 ± 0.006	101	−577	70
−48.88	6.120 ± 0.016	124	239	7
−44.31	1.714 ± 0.011	166	−30	17
−38.49	115.53 ± 0.09	114.0	70.0	2.0
−36.75	61.32 ± 0.05	61.0	−5.0	2.1
−34.23	2.468 ± 0.012	31	−89	12
−33.13	0.762 ± 0.008	−161	−27	26
−26.24	0.221 ± 0.010	219	−565	200
−23.13	2.679 ± 0.008	0	32	7
−22.04	1.312 ± 0.012	518	47	23
7.64	10.725 ± 0.023	−70	73	6

Note. — Column 1 is the LSR velocity of the component peak emission. Column 2 is the flux density of the component peak emission, with its 2σ uncertainty due to the rms of the map. This provides a relative flux uncertainty between components, whereas the absolute flux calibration uncertainty is $\simeq 10\%$. Columns 3 and 4 represent the positional offsets (in right ascension and declination, respectively) of each maser component with respect to the position of the radio continuum emission. Column 5 is the 1σ relative positional uncertainty of each maser component. The actual relative accuracy between a pair of components should be obtained by adding quadratically their corresponding values in this column.

be used to determine its nature.

We can immediately exclude that this object is a YSO. The position of I15103 in the IRAS and MSX two color diagrams is not consistent with that of an HII region (Suárez et al. 2009). Moreover, considering its strong obscuration at optical wavelengths, if it was a YSO embedded on the parental cloud it should show significant molecular line emission associated with the cloud. In practice, we should detect interstellar molecular line emission with an LSR velocity close to that of I15103, but this is not the case. The Red MSX survey (RMS) archive (Urquhart et al. 2007b; Lumsden et al. 2013) shows several interstellar components of ^{13}CO(J=1 → 0) (Fig. 3). None of these components is close to that of the star of $\simeq -23$ km s^{-1}, estimated from the maser position-velocity distribution (Fig. 2 and Section 3.2), which indicates that the object is not a YSOs. However, the velocity estimate from the maser distribution is indirect and somewhat uncertain.

A more direct estimate of the stellar velocity can be obtained from our Herschel data (Fig. 3). The CO(J=5 → 4) spectrum shows some narrow emission and absorption features of interstellar origin, whose velocities coincide with those in the ^{13}CO(J=1 → 0) spectrum. However, there is an additional broader, weak component between $V_{\rm LSR} \simeq -28$ and -8 km s^{-1}, close to the central velocity estimated from the maser distribution. This broad component clearly dominates the CO(J=10 → 9) emission, which traces hotter gas than the CO(J=5 → 4) line (i.e., presumably closer to the central star). There could still be some interstellar contamination in the CO(J=10 → 9) spectrum at $V_{\rm LSR} \simeq 0$ km s^{-1}, but there is obvious emission around $V_{\rm LSR} \simeq -20$ km s^{-1} which has no interstellar counterpart in the ^{13}CO(J=1 → 0) line. Assuming that the emission around 0 km s^{-1} is interstellar, the broad component would have a half-power width 20 ± 5 km s^{-1} (centered at -18 ± 3 km s^{-1}), which is significantly broader than the interstellar CO(J=5 → 4) and ^{13}CO(J=1 → 0) components, and is similar to the line widths observed in CO spectra of other water fountains (Imai et al. 2009, 2012; Rizzo et al. 2013), tracing the expansion of the circumstellar structure. We can conclude that this CO(J=10 → 9) emission is of circumstellar origin. The absence of significant interstellar ^{13}CO(J=1 → 0) molecular line emission associated with the source rules out its nature as a YSO.

Having established its evolved nature, its classification as a PN relies on the presence of ionized gas. This is in-

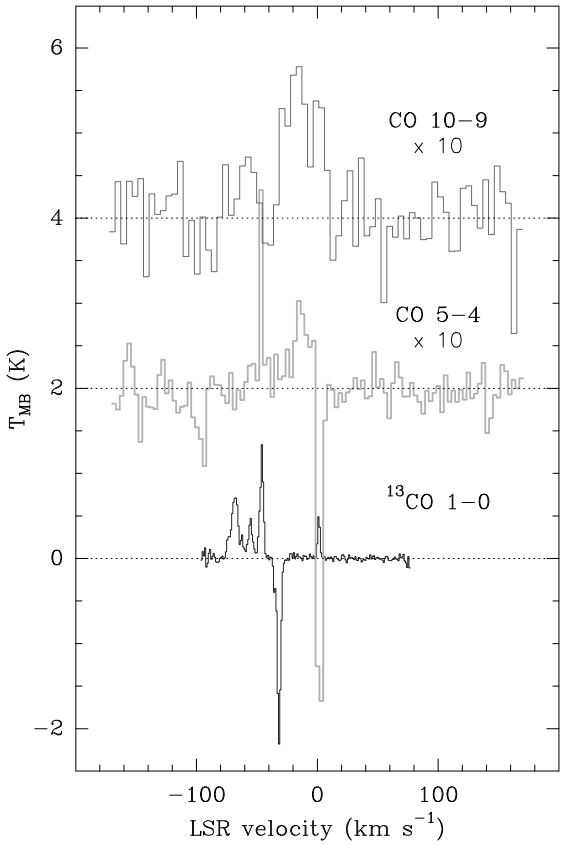

Figure 3. CO spectra toward IRAS 15103−5754. From top to bottom: CO(J=10 → 9) and CO(J=5 → 4) obtained with Herschel (this paper), and ^{13}CO(J=1 → 0) spectrum from the RMS survey (Urquhart et al. 2007b). The two Herschel spectra have been multiplied by 10 and shifted vertically, to improve their visualization

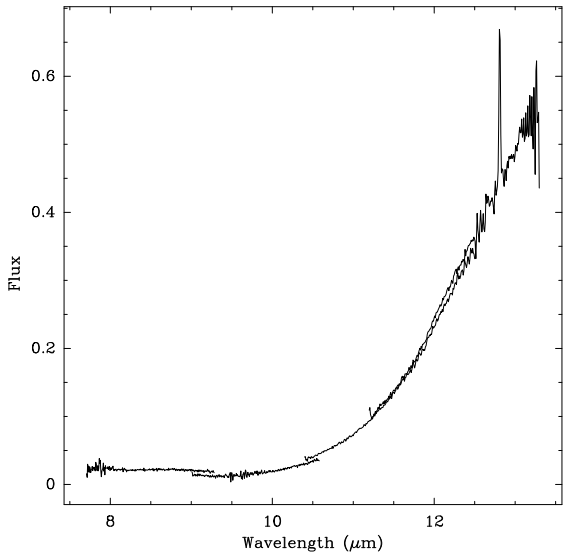

Figure 4. Mid-IR spectrum toward IRAS 15103−5754, obtained with VISIR instrument at the VLT . The flux is in arbitrary units. The [NeII] at 12.8 μm is clearly detected.

deed the case, since its IR spectrum shows a clear emission line of [NeII] at 12.8 μm (Fig. 4). Furthermore, the presence of [NeII] was also hinted at the mid-IR images presented in Fig B7 of Lagadec et al. (2011). The filter containing the [NeII] line is centered at 12.81 μm and has a width of 0.42 μm, whereas the SiC filter is at a nearby wavelength (11.85 μm), but it is ten times wider (2.24 μm) and therefore, significantly more sensitive for similar exposure times. However, note that the image in the narrower [NeII] filter seems more extended than that in the SiC one. After rescaling both images to get the same peak brightness, we confirmed that this extended emission in brighter in the [NeII] image. This is not expected if the emission in those filters is due to continuum alone, so the excess must be attributed to the [NeII] line emission. Those images suggest that [NeII] emission is diffuse and extended, as expected in a photoionized region.

3.4. *Comparison with other WFs and with water-maser-emitting PNe*

There is not a well-established definition of what a WF is. The first WFs were identified based on the extremely large velocity spreads in their water maser spectra ($>$ 100 km s^{-1} Likkel & Morris 1988; Imai et al. 2002, 2004). However, the velocity spread itself does not constitute a reliable criterion for definition, since it depends on the relative orientation with respect to the observer. Therefore, other objects with lower velocity spreads (e.g., $\simeq$ 50 km s^{-1} Boboltz & Marvel 2005) were later included in the WF category given their similarities with higher-velocity objects. Despite the lack of a clear-cut definition, the general trend is to consider a source as a WFs when its water maser emission traces collimated mass loss with velocities larger than that of the expansion velocities of the circumstellar envelopes in these objects (10-20 km s^{-1}, as traced by double-peaked OH spectra with separations of 20-40 km s^{-1} between the components, te Lintel Hekkert et al. 1989).

We also note that in AGB stars, the velocities of the H_2O maser components is always contained within the velocity range of OH maser emission. WFs show the opposite behavior, with some H_2O maser emission outside the velocity range of OH (Gómez et al. 1994). However, while this is a useful observational criterion to identify new WF candidates, it does not constitute a definition of WF itself. In the case of I15103, the only published OH spectrum is that obtained with the Parkes radio telescope by te Lintel Hekkert & Chapman (1996), which shows a single component at $\simeq -47$ km s^{-1}. Therefore, it is not possible to obtain an OH velocity range. Moreover, given the large beam of the Parkes antenna at 18 cm (half power beam width $\simeq 12.6'$), there is no guarantee that the OH emission actually arises from I15103.

Therefore, if we define a WF as an object whose water maser emission has a velocity spread larger than that of the typical AGB envelopes, and with this emission tracing collimated mass-loss, then I15103 is a WF as far as the definition goes. However, this source shows some differential characteristics with other WFs that are worth considering:

1. The water maser components in I15130 are present over the whole velocity range, without no clear clustering. The WFs IRAS 18296−0958 (Yung et al. 2011) and OH 009.1-0.4 (Walsh et al. 2009) also show a similar pattern in their spectra. However, most WFs show two groups of water maser components, clearly separated in velocity (e.g., Imai et al. 2002; Boboltz & Marvel 2005; Gómez et al. 2011), with a third central group at intermediate velocities in some objects (Imai et al. 2013). In the cases with clearly separated groups, the clusters at extreme velocities seem to trace the tips of a bipolar jet, and the central group could be an equatorial flow. However, in I15103 and the WFs with no clustering, the maser emission traces the mass loss along the whole body of the jet, not just the tips.

2. The "Hubble-flow" pattern in the position-velocity distribution of masers in I15130 (Fig. 2) is not clearly seen in any other WF, which suggest that the mass-loss process in this object may be of a different nature.

3. There is a clear bias in velocity, with most maser components being blueshifted with respect to the velocity of the central star. The result is that only the blueshifted side of the jet is clearly collimated. There are other WFs whose maser jet and/or the spectrum is also one-sided or strongly asymmetrical, such as IRAS 18460−0151 (Imai et al. 2013) or IRAS 15445−5449 (Bains et al. 2009), but most WFs are clearly bipolar. As mentioned in Sec. 3.2, a possible explanation for this bias is the presence of the radio continuum emission, which is amplified by the foreground (blueshifted) side of the jet by the maser mechanism.

All these differences with the properties of typical WFs suggest that while I15103 formally fulfil the criteria to be considered a WF, it has some unusual characteristics (although none of them are unique among WFs). Moreover, and what is probably more important, the discussion above also indicates that WFs show characteristics

that are very different from one another, and that they do not constitute an homogeneous group. We may have to consider revising the definition of what a WF is or, alternatively, to further subdivide this class into several subcategories according to their physical characteristics. The present category of WFs may in fact include several different types of objects that only share a common characteristic (the presence of collimated, high-velocity jets traced by water masers), but that might be fundamentally different otherwise.

I15103 is also one of the few PNe showing water maser emission (hereafter H_2O-PNe). This category of sources comprises a total of 5 confirmed members (Miranda et al. 2001; de Gregorio-Monsalvo et al. 2004; Gómez et al. 2008; Uscanga et al. 2014). We note, however, that the characteristics of the maser emission in I15103 is also significantly different from the other 4 H_2O-PNe. The velocity spread in the water maser emission in other H_2O-PNe is small (< 15 km s^{-1}), and most of the maser emission seem to trace equatorial tori around the central star. Only in the case of K3-35 (Miranda et al. 2001) some maser components may be related with a jet, but with a much lower velocity than in the case of WFs. Moreover, these components were transient and have not been observed thereafter (de Gregorio-Monsalvo et al. 2004).

In summary, although I15103 is formally both a WF and a H_2O-PN, there are significant differences with other members of these classes, and its mere inclusion in these categories should be taken with care. I15103 might be the first object of a completely different class of evolved object, whose physical characteristics might not be comparable with the rest WFs and H_2O-PNe.

3.5. *Evolutionary implications of the processes observed in IRAS 15103−5754*

Even though water maser emission is present in several PNe (Miranda et al. 2001; de Gregorio-Monsalvo et al. 2004; Gómez et al. 2008; Uscanga et al. 2014), the collimated high-velocity water maser emission that characterizes WFs have only been observed so far in late AGB and post-AGB stars. The presence of a collimated water maser outflow in this source suggests that I15103 is an extremely young PN, which is consistent with the results in Suárez et al. (2014), who suggested that newly started photoionization is changing the spectral index of its radio continuum emission.

As mentioned above, this source is also unique among WFs in the sense that its water maser emission shows a linear increase of velocity with distance from the central star (a so called Hubble flow). This kinematical pattern is expected in explosive or ballistic mass-loss events. In principle, one could speculate whether maser emission in all WFs have an explosive origin, but the Hubble flow would not be evident shortly after the mass-loss event. Only as the ejected material moves away from the star, the faster gas would move farther away, and a Hubble flow would become evident. The fact that I15103 is a PN, i.e., in a later evolutionary stage than all the other known WFs, would be consistent with this time evolution of the kinematical pattern.

However, we note that the main structure of water maser emission in I15103 follows a linear distribution, with no clear gap between the maser components and the central star, whereas most WFs show their maser emission clustered on two well-separated red- and blue-shifted groups detached from the star and on each side of it (e.g. Imai et al. 2002; Boboltz & Marvel 2005; Gómez et al. 2011). If this clustered distribution were due to a single explosive event, we could expect a Hubble flow to develop with time, but the gap between the maser emission and the central star would increase, and no emission would be detected close to the star. On the other hand, a few other WFs (Walsh et al. 2009; Yung et al. 2011) show a more extended water maser distribution, with components close to the star, but no clear Hubble-flow pattern is present. Therefore, the mass-loss processes that give rise to water maser emission in I15103 seem to be completely different from all the other known WFs. We suggest that water maser emission in WFs that are still in the post-AGB stage is pumped mainly by jets, and this emission is seen at the bow shock created by the jet (in the cases where there are two separate clusters of water masers) or along the body of the jet (if there is a more continuous maser distribution). However, as the star enters the PN phase, high velocity water maser emission traces singular explosive events. This would indicate a fundamental change of the mass loss process in evolved stars around the end of the post-AGB phase. This type of explosive event could be a common feature at the early stages of bipolar PNe, as evidenced by the occurrence of Hubble-like flows in these objects. The Hubble-flow pattern in I15103, however, is seen at a smaller scale ($\lesssim 850$ AU) than in other PNe and proto-PNe, and it shows a steeper velocity gradient. In particular, the Hubble flow in I15103 has a slope of $\simeq 150$ km s^{-1} arcsec^{-1}, while it is $\simeq 2.6$ km s^{-1} arcsec^{-1} in the PN NGC 6302 (Meaburn et al. 2008), which is at a similar distance (1.1 kpc). In the case of an explosive event, we expect this velocity gradient to decrease with time, since the ejected material will cover a larger spatial extension. The velocity pattern we see in I15013 could represent the earliest manifestations of explosive phenomena among PNe and its precursors.

4. CONCLUSIONS

We presented observations of radio continuum and water maser emission at 22 GHz, as well as submm CO and mid-infrared spectra of the source IRAS 15103−5754, a candidate PN where single-dish observations had previously revealed a water maser spectrum that suggested the presence of a WF outflow. Our main conclusions are as follow:

- Water maser emission shows a wide velocity spread of $\simeq 75$ km s^{-1}, and it is spatially associated with the radio continuum emission. Most of the water maser components are distributed following an elongated distribution, with an orientation similar to the nebula seen in the mid-IR, and tracing a collimated high-velocity outflow.

- IRAS 15103−5754 is confirmed as a PN, based on the absence of interstellar molecular emission close to the velocity of the source (thus, ruling out it is a YSO), and the presence of ionized material. The presence of a high velocity maser outflow indicates that the source is a WF, being the first known PN

belonging to this class of objects. All previously known WFs were late AGB or post-AGB stars.

- The velocity distribution of the maser emission shows a rough linear trend, with higher velocities farther away from the central star. Such a "Hubble-like" flow may be indicative of a short-lived, explosive event. This velocity pattern is not seen in other WFs, which are in previous evolutionary stages.

- We suggest that water maser emission in WFs that are still in the post-AGB stage is pumped mainly by shocks in jets. However, as the star enters the PN phase, high velocity water maser emission traces singular explosive events. This would represent an important change in the mass loss processes at the end of the post-AGB phase. The "Hubble flow" we detected at small scales ($\lesssim 850$ AU) could be the first manifestation of explosive events, which seem to be a common feature in the kinematics of more evolved PNe.

JFG wishes to express his gratitude to CSIRO Astronomy and Space Science, and the Observatoire de la Côte d'Azur for their support and hospitality during the preparation of this paper. JFG, OS, and LFM are supported by MICINN (Spain) grant AYA2011-30228-C03-01, while MAG is suported by grant AYA2011-29754-C03-02 (both grants include FEDER funds). JRR acknowledges support from MICINN grants CSD2009-00038, AYA2009-07304, and AYA2012-32032. LFM acknowledges partial support from grant 12VI20 of the Universidad de Vigo. LU is supported by grant PE9-1160 of the Greek General Secretariat for Research and Technology in the framework of the program Support of Postdoctoral Researchers. GRL acknowledges support from CONACyT and PROMEP (Mexico). This paper made use of information from the Red MSX Source survey database at http://rms.leeds.ac.uk/cgi-bin/public/RMS_DATABASE.cgi which was constructed with support from the Science and Technology Facilities Council of the UK.

Facilities: ATCA, Herschel, VLT .

REFERENCES

Akashi, M., & Soker, N. 2013, MNRAS, 436, 1961
Alcolea, J., Bujarrabal, V., Sánchez Contreras, C., Neri, R., & Zweigle, J. 2001, A&A, 373, 932
Bains, I., Cohen, M., Chapman, J. M., Deacon, R. M., & Redman, M. P. 2009, MNRAS, 397, 1386
Balick, B., Huarte-Espinosa, M., Frank, A., et al. 2013, ApJ, 772, 20
Boboltz, D. A., & Marvel, K. B. 2005, ApJ, 627, L45
Bujarrabal, V., Alcolea, J., Neri, R., & Grewing, M. 1997, A&A, 320, 540
Bujarrabal, V., Castro-Carrizo, A., Alcolea, J., & Sánchez Contreras, C. 2001, A&A, 377, 868
Caswell, J. L., & Green, J. A. 2011, MNRAS, 411, 2059
Corradi, R. L. M., & Schwarz, H. E. 1993, A&A, 269, 462
de Graauw, T., Helmich, F. P., Phillips, T. G., et al. 2010, A&A, 518, L6
de Gregorio-Monsalvo, I., Gómez, Y., Anglada, G., et al. 2004, ApJ, 601, 921
Dennis, T. J., Cunningham, A. J., Frank, A., et al. 2008, ApJ, 679, 1327
Desmurs, J.-F. 2012, IAU Symposium, 287, 217
Gómez, J. F., Suárez, O., Gómez, Y., et al. 2008, AJ, 135, 2074
Gómez, J. F., Rizzo, J. R., Suárez, O., et al. 2011, ApJ, 739, L14
Gómez, Y., Rodríguez, L. F., Contreras, M. E., & Moran, J. M. 1994, RMxAA, 28, 97
Hrivnak, B. J., Smith, N., Su, K. Y. L., & Sahai, R. 2008, ApJ, 688, 327
Imai, H. 2007, IAU Symposium, 242, 279
Imai, H., Obara, K., Diamond, P. J., Omodaka, T., & Sasao, T. 2002, Nature, 417, 829
Imai, H., Morris, M., Sahai, R., Hachisuka, K., & Azzollini F., J. R. 2004, A&A, 420, 265
Imai, H., He, J.-H., Nakashima, J.-I., Ukita, N., Deguchi, S., & Koning, N. 2009, PASJ, 61, 1365
Imai, H., Chong, S. N., He, J.-H., et al. 2012, PASJ, 64, 98
Imai, H., Deguchi, S., Nakashima, J.-i., Kwok, S., & Diamond, P. J. 2013, ApJ, 773, 182
Izzo, C., Kornweibel, N., McKay, D., et al. 2004, The Messenger, 117, 33
Lagadec, E., Verhoelst, T., Mékarnia, D., et al. 2011, MNRAS, 417, 32
Lagage, P. O., Pel, J. W., Authier, M., et al. 2004, The Messenger, 117, 12
Likkel, L., & Morris, M. 1988, ApJ, 329, 914
Lumsden, S. L., Hoare, M. G., Urquhart, J. S., et al. 2013, ApJS, 208, 11
Meaburn, J., López, J. A., Steffen, W., Graham, M. F., & Holloway, A. J. 2005, AJ, 130, 2303
Meaburn, J., Lloyd, M., Vaytet, N. M. H., & López, J. A. 2008, MNRAS, 385, 269
Miranda, L. F., Gómez, Y., Anglada, G., & Torrelles, J. M. 2001, Nature, 414, 284
Pilbratt, G. L., Riedinger, J. R., Passvogel, T., et al. 2010, A&A, 518, L1
Ramos-Larios, G., Guerrero, M. A., Suárez, O., Miranda, L. F., & Gómez, J. F. 2012, A&A, 545, A20
Reid, M. J., Menten, K. M., Zheng, X. W., et al. 2009, ApJ, 700, 137
Rizzo, J. R., Gómez, J. F., Miranda, L. F., et al. 2013, A&A, 560, A82
Roelfsema, P. R., Helmich, F. P., Teyssier, D., et al. 2012, A&A, 537, A17
Sahai, R., & Trauger, J. T. 1998, AJ, 116, 1357
Sault, B., & Killeen, N. 2004, The Miriad User Guide, http://www.atnf.csiro.au/computing/software/miriad/
Soker, N., & Kashi, A. 2012, ApJ, 746, 100
Suárez, O., García-Lario, P., Manchado, A., et al. 2006, A&A, 458, 173
Suárez, O., Gómez, J. F., & Miranda, L. F. 2008, ApJ, 689, 430
Suárez, O., Gómez, J. F., Miranda, L. F., et al. 2009, A&A, 505, 217
Suárez, O., Gómez, J. F., Bendjoya, Ph., et al. 2014, ApJ, submitted
te Lintel Hekkert, P., Versteege-Hensel, H. A., Habing, H. J., & Wiertz, M. 1989, A&AS, 78, 399
te Lintel Hekkert, P., & Chapman, J. M. 1996, A&AS, 119, 459
Urquhart, J. S., Busfield, A. L., Hoare, M. G., et al. 2007a, A&A, 461, 11
Urquhart, J. S., Busfield, A. L., Hoare, M. G., et al. 2007b, A&A, 474, 891
Uscanga, L., Gómez, J. F., Suárez, O., & Miranda, L. F. 2012, A&A, 547, A40
Uscanga, L., Gómez, J. F., Miranda, L. F., et al. 2014, MNRAS, 444, 217
van de Steene, G. C. M., & Pottasch, S. R. 1993, A&A, 274, 895
Vlemmings, W. H. T., Amiri, N., van Langevelde, H. J., & Tafoya, D. 2014, A&A, 569, AA92
Walsh, A. J., Breen, S. L., Bains, I., & Vlemmings, W. H. T. 2009, MNRAS, 394, L70
Yung, B. H. K., Nakashima, J.-i., Imai, H., et al. 2011, ApJ, 741, 94